PLOS CLIMATE

RESEARCH ARTICLE

Dust as a solar shield

Benjamin C. Bromley[1]*, **Sameer H. Khan**[1], **Scott J. Kenyon**[2]

1 Department of Physics and Astronomy, University of Utah, Salt Lake City, UT, United States of America, **2** Smithsonian Astrophysical Observatory, Cambridge, MA, United States of America

* bromley@physics.utah.edu

Citation: Bromley BC, Khan SH, Kenyon SJ (2023) Dust as a solar shield. PLOS Clim 2(2): e0000133. https://doi.org/10.1371/journal.pclm.0000133

Editor: Juan A. Añel, Universidade de Vigo, SPAIN

Received: August 30, 2022

Accepted: December 7, 2022

Published: February 8, 2023

Peer Review History: PLOS recognizes the benefits of transparency in the peer review process; therefore, we enable the publication of all of the content of peer review and author responses alongside final, published articles. The editorial history of this article is available here: https://doi.org/10.1371/journal.pclm.0000133

Data Availability Statement: The only actual data specific to our study is now available in S1 Table. We generate figures from the data in-core with Python scripts available now as a tar file in a new Github repository: https://github.com/benjbromley/Dust-as-a-solar-shield.

Funding: The University of Utah Office of Undergraduate Research provided a stipend to co-

Abstract

We revisit dust placed near the Earth–Sun L_1 Lagrange point as a possible climate-change mitigation measure. Our calculations include variations in grain properties and orbit solutions with lunar and planetary perturbations. To achieve sunlight attenuation of 1.8%, equivalent to about 6 days per year of an obscured Sun, the mass of dust in the scenarios we consider must exceed 10^{10} kg. The more promising approaches include using high-porosity, fluffy grains to increase the extinction efficiency per unit mass, and launching this material in directed jets from a platform orbiting at L_1. A simpler approach is to ballistically eject dust grains from the Moon's surface on a free trajectory toward L_1, providing sun shade for several days or more. Advantages compared to an Earth launch include a ready reservoir of dust on the lunar surface and less kinetic energy required to achieve a sun-shielding orbit.

Introduction

Climate change on Earth is an existential threat. Increased entrapment of solar energy, the result of changes in composition of the Earth's atmosphere, is acknowledged to be a severe problem [1–3]. One class of strategies for combating climate change is to reduce the solar irradiance by intercepting sunlight before it reaches Earth [4]. The target attenuation of sunlight, based on modeling, is approximately 1–2% [5, 6]. For historical context, aerosols in the Earth's atmosphere can potentially serve as light reflectors or absorbers that redistribute solar radiation [7]. However, their overall impact may be difficult to predict owing to uncertainties in how they may be circulated and their interaction with clouds. Regional weather changes, the nature of deployment programs, and long-term environmental effects will inevitably cause uneven society hardships and benefits, arguing that other approaches should be prioritized [8, 9].

Space-baced approaches for solar radiation management provide an alternative. Objects in space—a large screen [10–12] or a swarm of small artificial satellites [13, 14]—that are well-positioned at the L_1 Lagrange point between Earth and the Sun can efficiently shade our planet. Challenges includes maintaining orbits in the face of radiation pressure from sunlight. The optical properties of the orbiters are thus chosen to mitigate this problem. A high degree of forward scattering allows light to be deflected without transferring much photon momentum, a feat accomplished with refractive, non-absorbing material. A second challenge is that the amount of material required to provide climate-impacting shade exceeds 10^9 kg, which is

author SHK through the Undergraduate Research Opportunity Program (http://our.utah.edu/research-scholarship-opportunities/urop/). The funder(s) had no role in study design, data collection and analysis, decision to publish, or preparation of the manuscript.

Competing interests: The authors have declared that no competing interests exist.

roughly a hundred time more mass than humans have sent into space to date. However, strategies have been identified that are feasible [13].

Variations on the original proposals to shade Earth with artificial sun shields include the use of dust. Clouds of micron-size gains at the Earth–Sun L_1 point [15–17], at Lagrange points of the Moon-Earth system [11, 18], and in orbit around Earth [19–21] have all shown some promise, albeit with limitations. The potential sources of dust include terrestrial and lunar mines and near-Earth asteroids. In all cases, masses $\gtrsim 10^{10}$ kg are necessary to have climate impact.

Here, we revisit the reduction of sunlight received by Earth that results from the placement of dust at or near the inner Lagrange point, L_1, lying directly between Earth and the Sun, including gravitational perturbations from the Moon and other planets. While unstable, these corotating orbits allow for the possibility of temporarily shading Earth. We start by assessing the shadows produced by various types of dust; then we numerically determine orbits that persist near L_1, including the impact of radiation pressure and solar wind. Our main results are a connection between the quantity and quality of dust and the attenuation of sunlight at Earth on achievable orbits near L_1. To compare with previous work, we target a reduction in solar irradiance of 1.8%, or 6 attenuation-days per year.

Shading by dust near L_1

A particle orbiting the Sun can shield Earth by absorbing or scattering radiation. A shield's overall effectiveness depends on its ability to sustain an orbit that casts a shadow on Earth. In principle, a small shield placed at L_1 can remain in close alignment between Earth and the Sun, offering hope that it can provide steady sun shade. The distance between $L_1$and Earth, d_1, is approximately the Hill radius,

$$\mathrm{R_{Hill}} \equiv a_{\mathrm{semi}} \left(\frac{\mathrm{M}_\oplus}{3\mathrm{M}_\odot} \right)^{1/3} \approx 0.01 \text{ au}, \tag{1}$$

where a_{semi} is the semimajor axis of the Earth's orbit around the Sun, the masses $\mathrm{M}_\oplus$ and $\mathrm{M}_\odot$ correspond to Earth and the Sun, respectively, and 1 au $\approx 1.496 \times 10^{11}$ m. Knowing this distance allows us to estimate the effectiveness of a shield, whether it is a solid thin film or, as we consider here, a cloud of dust. The first step in this determination is how an individual dust grain interacts with sunlight.

Particle scattering

The amount of sunlight removed by a particle is quantified by a cross section, $Q_{\mathrm{ext}}\pi {r_p}^2$, where r_p is the particle's radius, and

$$Q_{\mathrm{ext}} = Q_{\mathrm{abs}} + Q_{\mathrm{sca}} \tag{2}$$

is the extinction efficiency factor, broken down in terms of absorption and scattering efficiencies (Q_{abs} and Q_{sca}, respectively). Light scattered by reflection and refraction is characterized by a phase function, $\Phi(\theta)$, giving the amount of incident light that is scattered at angle θ relative to the direction of travel of the incident beam. The anisotropy parameter,

$$g = \int \cos(\theta)\Phi(\theta)d\Omega / \int \Phi(\theta)d\Omega, \tag{3}$$

where the integration is over all solid angles, indicates whether light is, on average, back-scattered ($-1 \leq g < 0$), forward-scattered ($0 < g \leq 1$) or neither ($g = 0$, as for an isotropic

scattering). While the effectiveness of a particle as a sun shield is governed by Q_{ext}, the scattering anisotropy may also be important. A small particle that is impacted by radiation pressure feels a stronger force if it back-scatters photons, reversing their angular momentum, than if the particle forward-scatters them, with only modest changes to the flow of photon momentum [22].

Scattering outcomes depend strongly on particle size. For particles larger than a micron, bigger than the typical wavelength of sunlight, $\lambda \sim 0.5\ \mu$m, the scattering efficiency is $Q_{ext} \approx 2$; particles of this size block incident sunlight as a result of their geometric cross section A_p, equal to πr_p^2 for spheres, augmented by interference effects from their internal response to the incident radiation [23]. At distance d_1, the Earth-L_1separation, even objects as large as $\sqrt{\lambda d_1} \sim 10$ m will be in the Frauenhofer diffraction regime [24].

Particles with sub-micron radii are smaller than the typical wavelength of sunlight. The interaction of these small grains with light can be complicated, though the theories of Rayleigh, Lorentz, and Mie are powerful starting points. From Rayliegh theory, the efficiency factors for nanoparticles are

$$Q_{abs} \sim -\mathrm{Im}(K) r_p/\lambda \tag{4}$$

$$Q_{sca} \sim |K|^2 r_p^{\ 4}/\lambda^4, \tag{5}$$

where $K = (n^2 - 1)/(n^2 + 2)$ and n is the index of refraction. In this limit, scattered light is isotropic. For smaller particles in this regime, extinction efficiencies are low; for example, 0.01 μm silver nanoparties have $Q_{ext} \sim 0.01$ [25]. Small molecules, with physical radii of a few tenths of a nanometer and absorption cross sections typically smaller than 10^{-4} nm^2 when averaged across the solar spectrum, have extinction efficiencies below roughly 10^{-3}.

In the intermediate regime, where grains have radii of 0.1–1 μm, the extinction efficiencies are higher and admit the possibility of forward scattering. We use Mie theory to estimate scattering properties of these grains, incorporating the `miepython` package (`github.com/scottprahl/miepython`) to obtain average Q_{ext}, Q_{sca}, and g for particles of coal dust, sea salt, glass, and gold in sunlight, modelled with a blackbody spectrum running from 300 nm to 1500 nm. Table 1 provides a list of parameters.

Other dust or grain configurations include particles with elongated shapes (e.g., ice crystals) or in fluffy agglomerates. When the geometric limit applies, the average scattering cross section

Table 1. Optical properties.

material	density (kg/m^3)	refractive index
coal dust	1400	$1.8 - 0.2i$
sea salt	2000	$1.5 - 10^{-6}i$
glass	2500	$1.5 - 10^{-8}i$
lunar dust	2700	$1.7 - 10^{-3}i$
aluminum spheres	2700	$1.4 - 7.6i$
gold spheres	1930	$0.27 - 2.9i$

These values are intended only to be characteristic of the material listed. For lunar dust we adopt the characteristics of olivine, averaged over the solar spectrum [26].

https://doi.org/10.1371/journal.pclm.0000133.t001

of a randomly oriented, long cylinder (length L and diameter D) is

$$\frac{Q_{\text{ext}}(cyl)}{Q_{\text{ext}}(sph)} \approx 1.6\left(\frac{L/D}{10}\right)^{1/3}; (L \gg D \gg \lambda) \ . \tag{6}$$

When the wavelength of light is comparable to D, the cross-section is much larger [27].

Fluffy aggregates with high porosity may also increase the scattering efficiencies compared to objects with the same bulk composition and mass. The Bruggeman mixing rule allows for an estimate of n_{eff} the effective index of refraction of a non-absorbing composite material through the solution of

$$(1-f)\frac{1-n_{\text{eff}}^2}{1+2n_{\text{eff}}^2} + f\frac{n^2-n_{\text{eff}}^2}{n^2+2n_{\text{eff}}^2} = 0, \tag{7}$$

where f is the filling factor, defined to be a volume fraction of the aggregate material within the fluffy particle.

By varying composition and structure (shape, porosity), the optical properties of a material may be adjusted to optimize effectiveness as a solar shield.

Shadowing Earth

If a light-scattering particle lies directly between Earth and the Sun, it will diminish the solar irradiance at Earth by an amount that depends on its angular size, which depends on the cross-section and the distance from Earth [13]. In the limit where the particle is very close to Earth, just above the atmosphere for example, every photon scattered or absorbed by the particle would have hit Earth. The attenuation in sunlight, defined here as the fractional reduction of the total radiative power of the Sun received by Earth, is then the ratio of the cross-section of the particle to the area of the illuminated face of our planet. When the particle is farther from Earth, well beyond the L_1 point, its shadow, a penumbra, may extend beyond the Sun-facing disk of Earth. Many of the photons that the particle deflects would not have reached Earth. The attenuation in this case is comparatively small.

In general, the attenuation of solar irradiance at Earth, stemming from a particle with geometric cross section σ, is

$$\mathcal{A}_p = f_\bullet Q_{\text{ext}} \frac{\sigma}{\pi \mathrm{R}_\oplus^2} \tag{8}$$

where $f_\bullet$ is the fraction of solar photons deflected by the particle that would have otherwise reached Earth. This "shadowing efficiency" quantifies the effects of geometry, specifically the fraction of the particle's penumbral shadow that is occupied by the Sun-facing disk of Earth.

Toward estimating $f_\bullet$, we define $R_\bullet$, the radius of the particle's penumbra when projected onto the surface of a sphere about the Sun that contains the center of Earth:

$$R_\bullet \equiv \mathrm{R}_\odot d_p/(a_{\text{semi}} - d_p), \tag{9}$$

where a_{semi} is the Earth–Sun distance, and d_p is the distance from the Earth's center to the particle. Close to Earth, $R_\bullet$ is small, and grows as the particle is moved toward the Sun. At some optimal distance from Earth,

$$d_\bullet \approx a_{\text{semi}}\,\mathrm{R}_\oplus/(\mathrm{R}_\odot + \mathrm{R}_\oplus) \approx 0.91\ d_1 \tag{10}$$

the penumbra exactly covers the Sun-facing disk of Earth. As in the rightmost expression in the equation, $d_\bullet$ is curiously close to the distance between Earth and L_1, $d_1 \approx \mathrm{R}_{\text{Hill}}$ [13].

When Earth, the Sun, and a light-scattering particle are not aligned, the center of the penumbral shadow of the particle will fall some distance from the center of the Earth's Sun-facing disk given by

$$b = \frac{1}{a_{\text{semi}}} \left| \vec{d}_p \times \vec{a}_{\text{semi}} \right|, \tag{11}$$

where $\vec{d}_p$ is the particle position relative to Earth, and $\vec{a}_{\text{semi}}$ is the Earth's displacement from the Sun. With these definitions, the shadowing efficiency is

$$f_\bullet(d_p, b) = \begin{cases} 0 & (b > R_\bullet + \mathrm{R}_\oplus; \text{no shadow}); \\ \max(1, \mathrm{R}_\oplus^2 / {R_\bullet}^2) & (b < |R_\bullet - \mathrm{R}_\oplus|; \text{complete shadow}); \\ \{\mathrm{R}_\oplus^2 \cos^{-1}\left(\dfrac{b^2 + \mathrm{R}_\oplus^2 - {R_\bullet}^2}{2b\mathrm{R}_\oplus}\right) + {R_\bullet}^2 \cos^{-1}\left(\dfrac{b^2 + {R_\bullet}^2 - \mathrm{R}_\oplus^2}{2bR_\bullet}\right) + \\ \quad -\dfrac{1}{2}[(b + \mathrm{R}_\oplus + R_\bullet)(b - \mathrm{R}_\oplus + R_\bullet) \times \\ \quad (b + \mathrm{R}_\oplus - R_\bullet)(\mathrm{R}_\oplus + R_\bullet - b)]^{1/2}\Big\} / \pi {R_\bullet}^2 & (\text{otherwise}). \end{cases} \tag{12}$$

When a light-scattering particle is interior to $d_\bullet \approx 0.008$ au and aligned with Earth and the Sun. the shadowing efficiency is unity. Further out, at L_1 ($b \leq R_\bullet - \mathrm{R}_\oplus$, $f_\bullet \approx 0.82$). To estimate the impact of dust on the solar radiance, we consider the attenuation from a spherical particle with a radius of 1 μm, located at L_1 and aligned with Earth and the Sun:

$$\mathcal{A}_p \approx 2.0 Q_{\text{ext}} \left[\frac{r_p}{1\ \mu\text{m}}\right]^2 \times 10^{-26} \quad (\text{at } \mathrm{L}_1) \tag{13}$$

While this value is small for an individual absorbing particle, a substantial ensemble of dust particles may have a significant impact on the solar radiation received on Earth. If the particle were moved toward the Sun to a new distance $d_p > d_1$, then the attenuation would fall off roughly as the square of d_p. This decrease with distance may be an important consideration when establishing a swarm of particles at some new L_1 point in response to non-gravitational forces like radiation pressure.

A scatterer near L_1 in line with Earth and the Sun attenuates solar radiation by deflecting light out of the narrow cone aimed at the illuminated face of Earth. Light scattered into this cone, with a solid angle $\Delta\Omega$, amplifies the sunlight received by Earth by a factor

$$\mathcal{B} \approx \pi \frac{{r_p}^2}{{d_p}^2} \langle \Phi(\theta) \rangle|_{\Delta\Omega}, \tag{14}$$

where angular braces denote the phase function averaged over solid angle $\Delta\Omega$ in the Earth's direction. For a particle near L_1, aligned between Earth and the Sun, Earth appears as a disk with an angular radius of $\Delta\Theta = \mathrm{R}_\oplus / d_1 \approx 0.24^\circ$, filling a solid angle of $\Delta\Omega \approx 5.7 \times 10^{-5}$ steradians; the phase function in this case is evaluated around a scattering angle of 0°. In practice we estimate the average value of the phase function in $\Delta\Theta$ using the `miepython` routine `i_unpolarized` and a 7-point Simpson's 3/8s rule integrator, since the phase function can be sharply peaked at $\theta = 0^\circ$. For micron size grains at L_1, the amplification is generally below 0.1% of the level of the attenuation, even for strongly forward-scattering particles ($g \gtrsim 0.8$).

For larger particles with $r_p \gtrsim 10\ \mu$m, the phase function is so sharply peaked at $\theta = 0^\circ$ that the amplification can exceed over 10% of the magnitude of attenuation.

Particles that forward-scatter light amplify the sunlight received on Earth even when they provide no shade at all. While the magnitude of the effect is small compared with attenuation, an accumulation of dust particles just beyond the disk of the Sun from the Earth's perspective could overwhelm the impact of attenuation by those orbiting in front of the Sun. It is important to avoid a situation where a significant mass in dust lingers just outside the solar disk, brightening the terrestrial sky. Two factors mitigate this risk. First, as particles move away from alignment with Earth and the Sun, the scattering angle toward Earth increases, typically leading to a drop in the amplification. Second, particles displaced from L_1 tend to move away from that point quickly as compared with the metastable orbits at the Lagrange point. It seems unlikely to accumulate much dust in the broad space between Earth and the Sun.

Clouds of dust

A swarm of purely absorbing dust particles could provide an effective sun shield [15, 16, 19]. However, with an attenuation of solar radiation by a factor of 10^{-26} per micron-sized grain, climate-impacting reduction in solar radiance at Earth requires a large cloud of dust. To estimate the amount of material required to achieve Earth-climate impact, we first analyze a face-on, disk-like cloud with a radius R_{cloud}, depth Z in the Earth–Sun direction, and dust uniformly distributed within it with number density n. The cloud's optical depth along a path perpendicular to the disk is

$$\tau(R_\perp) = \begin{cases} Q_{\text{ext}} A_p n Z & (R_\perp < R_{\text{cloud}}) \\ 0 & (\text{otherwise}) \end{cases} \tag{15}$$

where $R_\perp$ is the path's distance from the cloud's central axis. When the cloud lies on the Earth–Sun axis, directly above the Earth's subsolar point, its attenuation is

$$\mathcal{A} = F(R_{\text{cloud}})[1 - \exp(-\tau)] \frac{{R_{\text{cloud}}}^2}{{d_1}^2} \frac{a_{\text{semi}}^2}{\text{R}_\odot^2} \quad (\text{on} - \text{axis disk}) \tag{16}$$

where

$$F(X) = \frac{1}{\pi X^2} \int_0^X 2\pi x f_\bullet(x) dx \tag{17}$$

is a measure of the average shadowing fraction provided by the penumbra of the disk. If the disk is comparatively small, so that $R_{\text{cloud}} \leq R_\bullet(1 - d_1/a_{\text{semi}}) \approx 650$ km, Earth lies within the penumbra of the entire cloud. Then, $F \approx 0.82$, its maximum value.

For Earth-climate impact, $\mathcal{A} \approx 1.8\%$. An optically thick cloud ($\tau \gg 1$), provides this level of shade when its physical radius is

$$R_{\text{cloud}} \approx 940 \text{ km} \quad (\text{ECI shield radius at } L_1); \tag{18}$$

For comparison, a disk radius of about 7000 km is required to totally eclipse the Sun from the perspective of the Earth's subsolar point. If a 940-km "cloud" were instead a sheet of aluminum with a thickness of 100 nm and areal density of 0.3 g/m^2, as in the insulating films on current spacecraft, the total mass would be 7.6×10^8 kg, equivalent to a sphere of about 40 m in radius. For structural support, though, the films on existing and proposed spacecraft have areal densities over an order of magnitude higher [13, 14].

An optically thin disk with a larger radius, for example 1500 km, requires

$$M_{\text{cloud}} = 1.6 \times 10^9 \left[\frac{Q_{\text{ext}}}{2}\right]^{-1} \left[\frac{\rho_p}{2.7\ \text{g/cm}^3}\right] \left[\frac{r_p}{1\ \mu\text{m}}\right] \text{kg} \quad (\text{at } L_1) \tag{19}$$

where the numerical value of the bulk density ρ_p applies approximately to both aluminum and silicate dust, and the scattering efficiency has a strong dependence on material properties and particle radius, r_p. At 1 μm, both aluminum and silicate grains have a high scattering efficiency ($Q_{\text{ext}} \gtrsim 2$ based on Mie scattering), and have similar mass requirements to reach the same attenuation target. Because aluminum is strongly absorbing, its extinction efficiency remains near $Q_{\text{ext}} = 2$ even when the grain size is reduced to 0.1 μm, cutting the required cloud mass by a factor of ten. By comparison, the extinction efficiency of silicate dust with $r_p = 0.1$ μm is only 0.7, reducing M_{cloud} by a factor of four. Coal dust is promising, as its density is comparatively low, yet like aluminum, it is absorbing and so retains a fairly high extinction efficiency ($Q_{\text{ext}} \approx 1.2$ for grain radii of 0.1 μm). A cloud of coal dust would require a mass of 1.3×10^8 kg to have climate impact. Modifications to grain porosity and shape can also increase the attenuation per unit mass. Fig 1 illustrates these dependencies.

As in the figure, the peaks of the attenuation curves for spherical particles as a function of grain size are fairly sharp at just under a micron for most of the materials considered. This result provides a guide to how dust might be mined, sifted or milled to achieve a desired level of attenuation, especially for natural materials that have a broad size distribution. Particle shapes of also impact attenuation by allowing more massive grains with elongated or porous configurations to scatter sunlight more effectively. Since more massive dust particles are less susceptible to the effects of radiation pressure and the solar wind, there may be a benefit to producing dust clouds with these "designer" materials, as discussed below. Production and delivery costs would differ, also impacting the feasibility of each grain type as a solar shield.

The attenuation calculations illustrated in Fig 1 assume that the cloud of dust is located at L_1. Non-gravitational forces (e.g., radiation pressure) may prevent the cloud from maintaining a stable position, although a sustained L_1-like orbit maybe be possible further away from Earth. If the distance between a cloud and Earth were increased beyond 1 R_{Hill}, yet retains alignment with the Sun so that Earth is fully in the penumbral shadow, then $f_\bullet$ falls off roughly as the square of

$$f_\bullet(0) \approx 0.82 \left[\frac{d_p}{0.01\ \text{au}}\right]^{-2} \quad (d_p \geq d_\bullet); \tag{20}$$

This value and the corresponding averaged shading factor F in Eq (3) generally diminish with increasing distance beyond L_1. We consider detailed grain orbits next.

Orbits near the L_1

Earth, on its orbit about the Sun, can gravitationally shepherd small bodies around it at distances well beyond the Moon. The spatial extent of its influence is characterized by the Hill radius (Eq (1)), On the line segment connecting Earth and the Sun, approximately one Hill radius away from Earth, is the Lagrange point, L_1; at that location, the inward force from the Sun is weakened by the outward pull of Earth in just the right amount so that an object there corotates with Earth, holding a position directly in between Earth and Sun.

Orbits at the Lagrange point L_1 are metastable. A well-placed test particle in an idealized restricted three-body experiment with Earth and Sun can orbit at L_1 for multiple dynamical times. However, numerical experiments demonstrate that finding the location of L_1 may

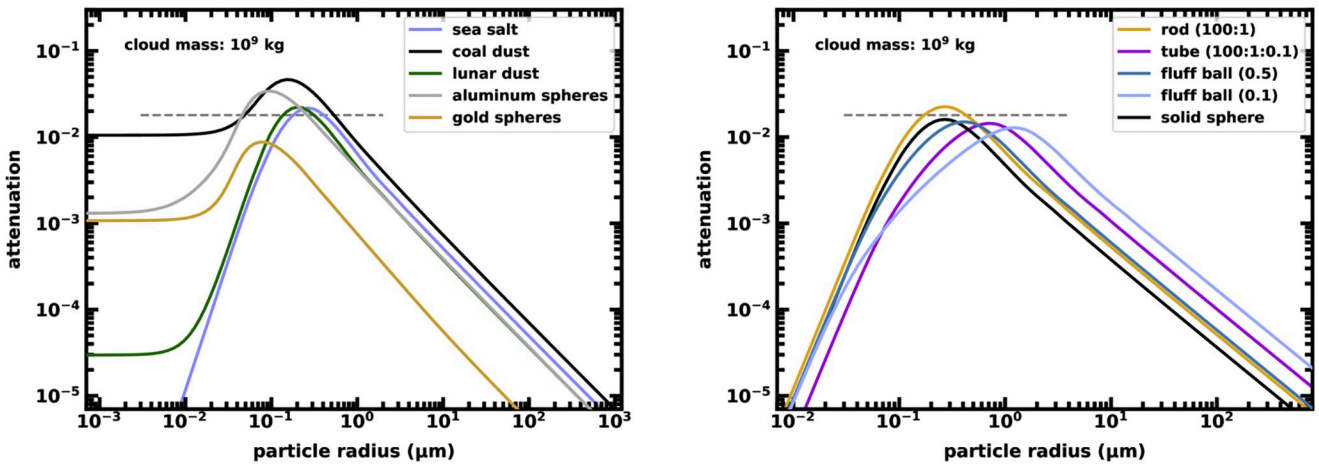

Fig 1. The attenuation from a monodisperse cloud of particles with total mass $M_{cloud} = 10^9$ kg at true L_1 as a function of radius. The left panel shows the attenuation for spherical particles of different types of material. The right panel illustrates the attenuation for dust made of glass but with different shapes, as in the legend. The horizontal axis in the right panel for glass particles is the volume equivalent radius. The shaped glass is (i) a cylindrical rod, with the length-to-diameter ratio as in the legend, (ii) a cylindrical tube with the given length:diameter:wall-thickness ratios; and (iii) "fluffy" spherical grains with the listed filling factors, so that (for example) 0.1 means 10% glass and 90% air bubbles or vacuum. The attenuation from spherical glass beads is shown for reference.

https://doi.org/10.1371/journal.pclm.0000133.g001

require fine tuning. Objects with starting positions that are separated from the L_1 location by less than a kilometer drift to distances of 1000 km or more from that point in less than a year. Velocity perturbations as small as a centimeter per second can also cause substantial drift away from L_1 in a dynamical time.

The Moon further complicates this picture. Together, Earth and the Moon are a binary system with a mass ratio near 0.012 and a separation of about a quarter of the Earth's Hill radius. Their relative motion produces a time-varying gravitational potential, where no physical orbit exactly follows a single point on the line connecting Earth and the Sun. We can nonetheless numerically find orbits that minimally drift from this line. Starting with Solar System data from JPL Horizons for the masses, locations and velocities of Earth, the Moon, Sun, Venus, Mars, Jupiter and Saturn, we use a sixth-order *n*-body integrator from the Orchestra code [28] to follow the orbits of massless tracer particles near the Earth–Sun L_1. Validation tests for the algorithm include energy conservation and phase-space convergence tests [29]. Here, energy is conserved to 1 part in 10^{14}; positions over the course of a one-year integration vary by less than about 10 km for orbits near the (metastable) Lagrange point. Increasing the time resolution of the code does not affect the results reported here.

To identify starting conditions in our simulations, we vary the initial displacement and velocity vectors, seeking an orbit that minimizes the r.m.s. distance of a tracer from the line connecting Earth and the Sun. Fig 2 illustrates the outcome, an L_1-tracking orbit that keeps an object within the disk of the Sun as seen from Earth, at least at the point where the Sun is directly overhead. S1 Table contains starting conditions for this and other simulations used here.

The numerical experiment in Fig 2 illustrates the existence of orbits that can provide sunshade over the course of a year and potentially longer. It also reveals that particles on these orbits drift around enough so that Earth does not always remain fully within their penumbra. The shadow fraction $f_\bullet$ falls from 0.82 for optimal alignment at L_1 to an average value of 0.60.

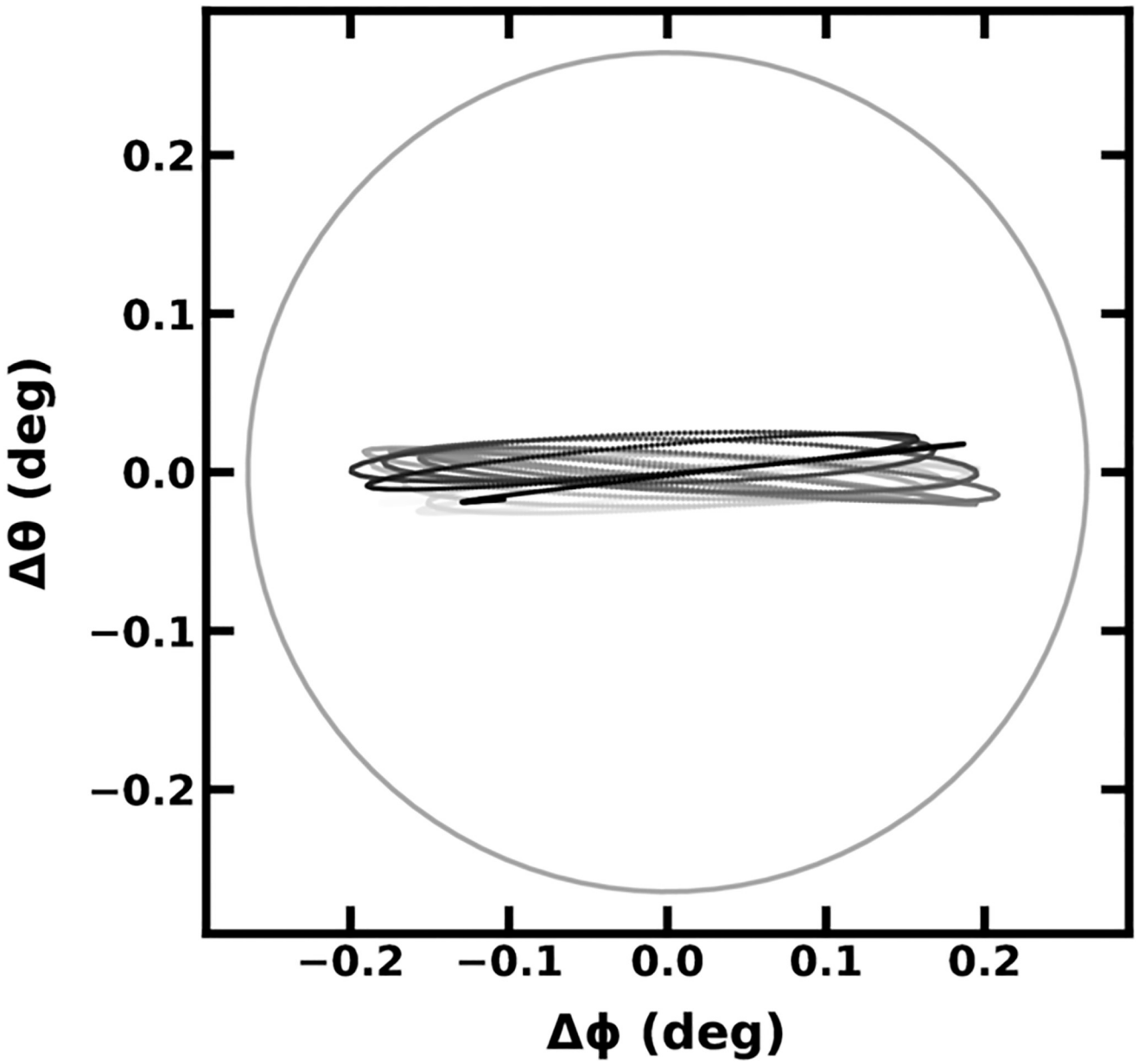

Fig 2. Location of a test particle on the face of the Sun as seen from Earth. The viewing location is the subsolar point. The plot axes are the angular displacement from the center of the Sun in the plane of the sky. The azimuthal direction is in the Earth's orbital plane, with Earth moving to the right. The starting date in the simulated experiment is April 20, 2022 (JD 2459699.500800758). A 6th-order symplectic integrator with took 4000 time steps to track the orbit over the course of one year. In the plot, the grey scale correlates with run time; earlier times have lighter shade.

https://doi.org/10.1371/journal.pclm.0000133.g002

Our simulations are limited to one year and rely on fine tuning of initial conditions. In real systems where non-gravitational forces are at play, or where ideal orbits are not initially achieved, some orbit corrections may be necessary to keep an object near L_1. The International Sun-Earth Explorer 3, the first satellite to occupy an orbit near L_1, like the others that followed it, occasionally maneuvered to stay in place. The solutions we find are no exception. Small corrections would be needed to keep a body near L_1 over multiple years. Next, we explore the role of non-gravitational forces in orbital dynamics.

Non-gravitational forces

Radiation pressure, Poynting-Robertson drag, and the solar wind contribute to the orbital dynamics of micron- and submicron-size particles [22, 30–32]. The acceleration of a single dust grain from these effects is

$$\frac{d\vec{r}_{\rm ng}}{dt} = \frac{L_\odot Q A_p}{4\pi c r^2 m_p}\left\{\left[1 + \frac{\eta}{Q}\frac{u}{c} - \left(1 + \frac{\eta}{Q}\right)\frac{\vec{v}\cdot\hat{r}}{c}\right]\hat{r} - \left(1 + \frac{\eta}{Q}\right)\frac{\vec{v}}{c}\right\} \tag{21}$$

where $L_\odot$ is the luminosity of the Sun, particle position $\vec{r}$ and velocity $\vec{v}$ as well as $u \approx 450$ km/s, the speed of the solar wind, are relative to the Sun, c is the speed of light, Q is an efficiency factor for radiation pressure, and $\eta \approx 1/3$ is the strength of corpuscular pressure from the solar wind relative to radiation pressure [22, 32]. The efficiency factor encodes the physics of scattering and absorption:

$$Q = Q_{\rm abs} + (1 - \langle\cos\theta\rangle)Q_{\rm sca}; \tag{22}$$

where the first term on the right is the fraction of radiation that is absorbed by the particle and the second term takes into account scattering. If light is completely back-scattered, $\langle\cos\theta\rangle \equiv g = -1$, hence $Q = 2Q_{\rm sca}$. When light is totally forward scattered ($g = 1$), Q is zero; radiation passes right through the particle [22].

Radiation pressure and the solar wind can strongly modify the orbits of small particles. The dominant term in Eq (21) is the radial, velocity-independent force of radiation pressure from the Sun. By convention, the parameter

$$\beta \equiv \frac{L_\odot Q A_p}{4\pi G c m_p M_\odot} \tag{23}$$

$$\approx 0.213\, Q\left[\frac{\rho_p}{2.7\ \mathrm{g/cm^3}}\right]^{-1}\left[\frac{r_p}{1\ \mu\mathrm{m}}\right]^{-1} \quad \text{(spheres)} \tag{24}$$

indicates the strength of this force compared to the Sun's gravity. Because radiation pressure depends on the flux of sunlight, $\sim L_\odot/r^2$, β depends on grain properties and not heliocentric distance. Thus, for $\beta < 1$, a grain orbits in a central force that still varies as $1/r^2$, although with diminished strength as the Euler constant $GM_\odot$ becomes $GM_\odot(1 - \beta)$. For $\beta \geq 1$, dust grains are ejected from the solar system.

For particles initially orbiting at the L_1 point, a non-zero β can lead to a rapid drift from the ideal, purely gravitational orbit. We define a persistence time,

$$T_{\rm per} = \frac{1}{f_\bullet(0)}\int f_\bullet(\vec{r}, t)\, t\, dt, \tag{25}$$

to represent the equivalent time that Earth is fully shaded by a grain. Fig 3 illustrates how the persistence time depends on β for spherical grains with several different radii. At small β, and for particles with radii much larger than a micron, the persistence time is long, at least months. Sub-micron grains have short persistence even when β is small, since they are swept away from L_1 by the solar wind.

We can increase persistence by noting that the reduction of the strength of the central force when $0 < \beta < 1$ means that Earth can shepherd dust at an "L_1-like" point closer to the Sun. An estimate of the distance between Earth and this new, size-dependent L_1 is derived from

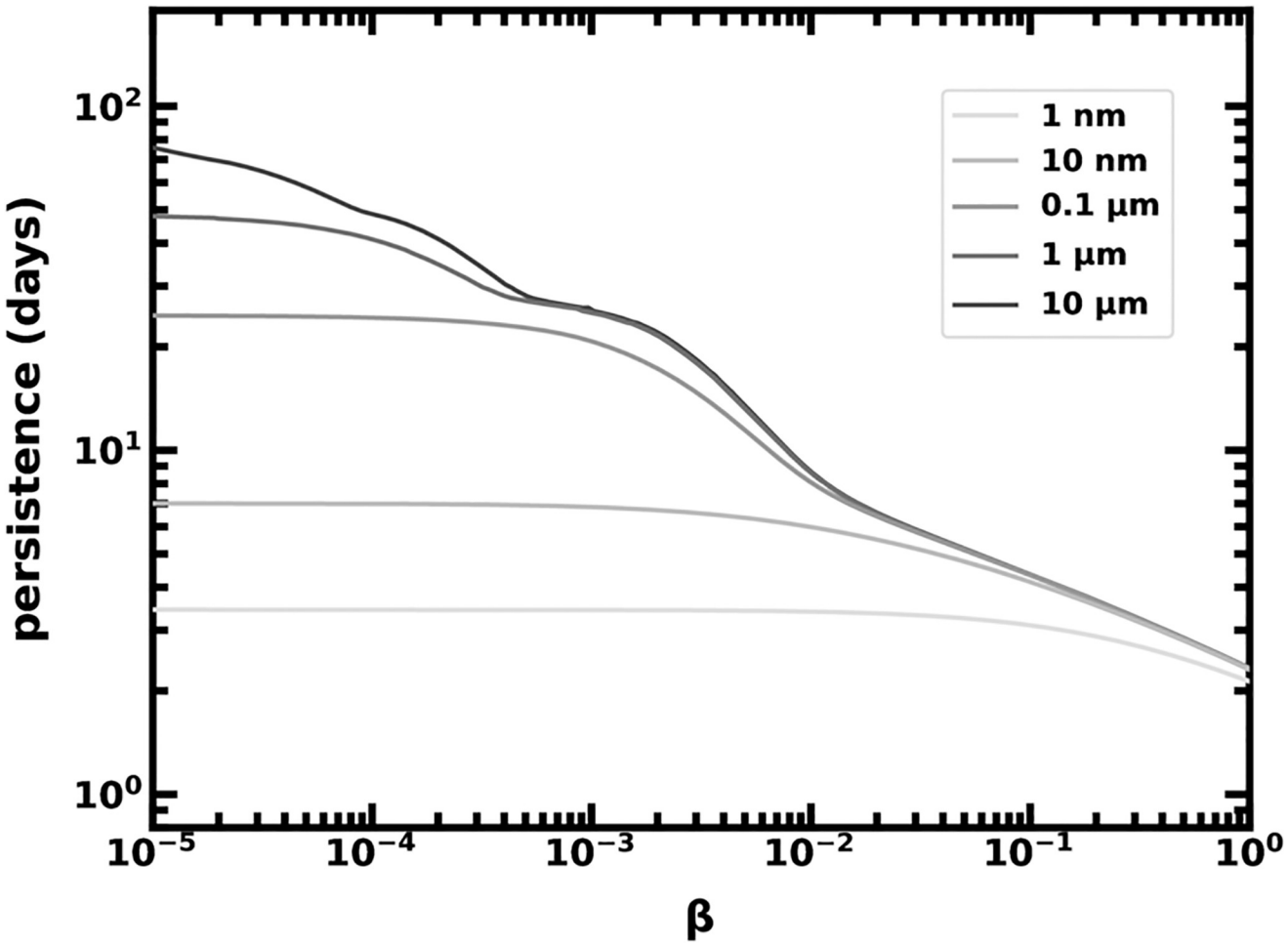

Fig 3. The persistence of spherical grains (ρ_p = 2.7 g/cm^3) at L_1 in the presence of non-gravitational forces. The various tracks show the persistence time for grains of difference sizes, as indicated in the legend. These values were obtained by numerical integration, where each grain was starting as in the trajectory in Fig 2. The overall trend is for persistence to increase with decreasing β, except at small β and for small grain radii. In these limits, the solar wind sweeps particles away from L_1.

https://doi.org/10.1371/journal.pclm.0000133.g003

equating the orbital speed of Earth with that of a dust particle on an inner orbit:

$$\frac{GM}{a_{\text{semi}}^3} = \left[\frac{(1-\beta)GM_\odot}{(a_{\text{semi}}-x)^2} - \frac{GM_\oplus}{x^2}\right]\frac{1}{M_\odot a_{\text{semi}}/M - x}, \tag{26}$$

where $M = M_\odot + M_\oplus$. For $\beta \leq 0.1$, the solution to the above equation is well-approximated by

$$d_p(\beta) \approx d_1 + 0.1047\beta + 1.6215\beta^2 \quad (\beta \lesssim 0.1). \tag{27}$$

We numerically determined the location of these L_1-like points, which can be several times more distant from Earth than "true L_1". Fig 4 provides examples. We verified that particle orbits may be sustained there for at least one year, balancing gravity, radiation pressure and solar wind in the ideal case when all quantities are constant.

The next step is to combine the orbits described in this section with the physics of dust scattering discussed earlier.

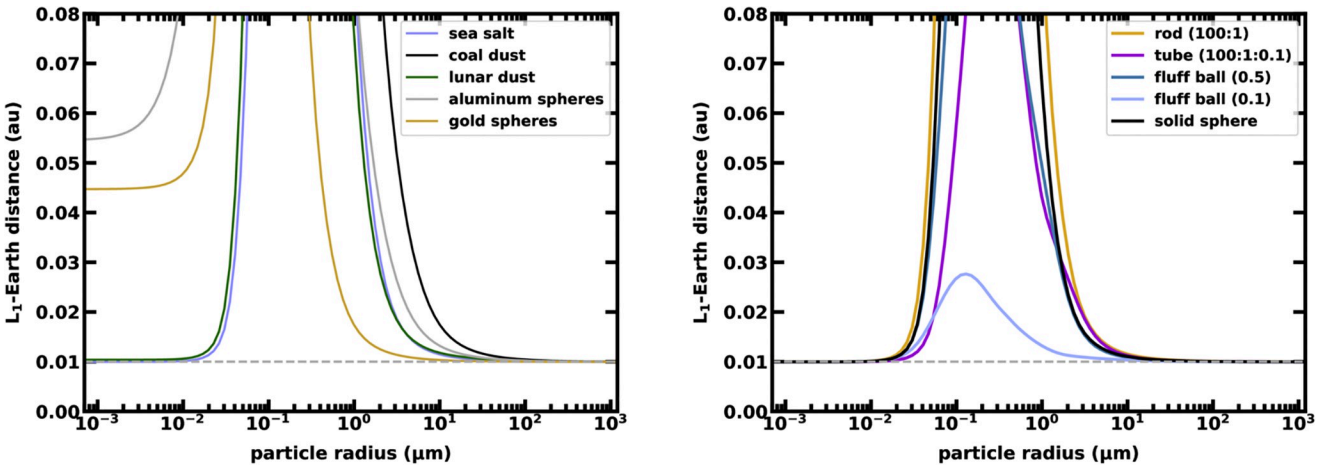

Fig 4. The distance of L_1-like orbits from Earth as a function of volume-equivalent radius for various grain types. When scattering is efficient, outwardly directed non-gravitational forces—radiation pressure and solar wind—oppose the force of gravity from the Sun. Then, Earth shepherds grains on L_1-like orbits at a greater distance. For most micron-size grains, though, the effect of radiation pressure is so strong that L_1-like orbits are well beyond ten Hill radii, and may not be achievable in the presence of other planets in the solar system.

https://doi.org/10.1371/journal.pclm.0000133.g004

Attenuation of sunlight by clouds of dust

A cloud at L_1

We first consider a monodisperse dust cloud at true L_1, as in Fig 2. The optimal attenuation for a cloud perfectly centered between Earth and the Sun is

$$\mathcal{A}_0 = f_\bullet(0)\,\frac{3Q_{\rm ext}M_{\rm cloud}}{4\pi\rho_p r_p d_1^{\,2}}\,\frac{a_{\rm semi}^2}{\mathrm{R}_\odot^2}, \tag{28}$$

where r_p, ρ_p, and $Q_{\rm ext}$ are the radius, bulk density and scattering efficiency of individual dust grains, respectively. Fig 1 provides examples of the attenuation as a function of dust particle size for a variety of materials. Coal dust, which is an efficient absorber, provides the strongest attenuation when dust particles are approximately a few tenths of a micron in radius. Glass, when formed into elongated, hollow tubes, has a peak attenuation when the volume-equivalent radius is about ten microns.

When providing shade to Earth, both the attenuation and the persistence of each grain at L_1 matter. A simple measure of this joint effect, the cumulative attenuation defined as $T_{\rm per} \times \mathcal{A}_0$, gives an estimate of the effectiveness of a grain type and quantity for impacting Earth climate. For example, a ten-year reduction of sunlight at Earth equivalent to the Maunder Minimum would have a value of 0.025 attenuation-years, or about 9 attenuation-days. For comparison, Fig 5 shows the cumulative attenuation for 10^9 kg of of dust composed of materials listed in Table 1. Coal dust with radii near 0.1 μm is most effective, in part because of its low density and high scattering efficiency. With a maximum cumulative attenuation of 0.03 days, approximately 300 times more dust of this size and composition ($\sim 1.5 \times 10^{11}$ kg) would need to be delivered to L_1 to reproduce the Maunder Minimum.

For context, 10^{11} kg of materials considered here would fill a sphere with a radius of roughly 200 m, comparable to the amount of material excavated per year in a single open-pit mine. The total mass launched into space over human history is considerably less, with estimates under 2×10^7 kg.

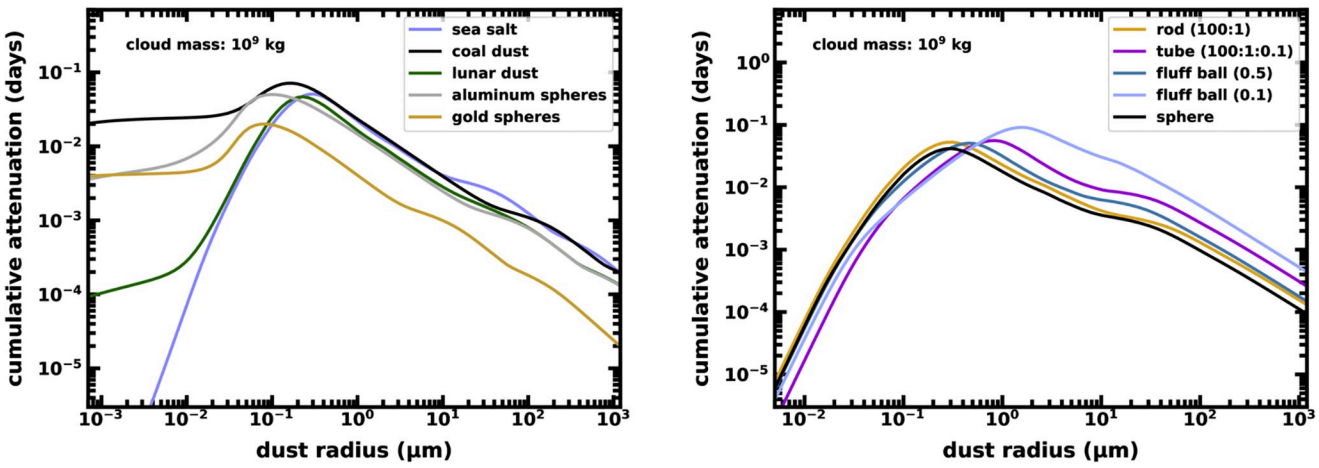

Fig 5. The cumulative attenuation from a monodisperse cloud of particles with total mass $M_{\text{cloud}} = 10^9$ kg at true L_1. The panels and curves in this figure correspond to those in Fig 1, except here, each point represents the attenuation times the persistence time (e.g., Fig 3).

https://doi.org/10.1371/journal.pclm.0000133.g005

Dust streamed from L_1

We ran simulations of fluffy glass aggregate particles with a volume-equivalent radius of 2 μm and filling factor of 0.1, launched from a platform on the L_1 orbit in Fig 2. We assessed two scenarios: (i) release all the particles at the start from L_1 with some small velocity dispersion (σ_v = 10 cm/s), and (ii) launching them from that same platform continuously over a one-month period in a directed jet. In the first case, the cumulative attenuation is about 0.085 days with a 10^9 kg cloud of dust; it is short because radiation pressure causes individual grains to drift from disk of the Sun. In the second case, this same cloud is launched with a velocity dispersion of 10 cm/s within a jet of mean speed 10 m/s directed at an angle $\theta_v = 65^\circ$ relative to the Earth's direction of travel. The persistence is approximately doubled, increasing to 0.15 days, since the jetted particles have initial speeds that compensate for the drifting motion away from the solar disk. Fig 6 is a snapshot of a particle jet launched in this way.

L_1-like orbits

With the possibility that dust can orbit at an L_1-like point more distant than true L_1 when it experiences non-gravitational forces, we introduce a second base-line attenuation factor for an optically thin, monodisperse cloud of dust with a total mass M_{cloud}:

$$\mathcal{A}_\beta = f_\bullet(0)\,\frac{3Q_{\text{ext}}M_{\text{cloud}}}{4\pi\rho_p r_p \mathrm{R}_\oplus^2} \tag{29}$$

where d_p is the distance between Earth and the cloud's location at the corotating, L_1-like point. We assume perfect alignment between the Sun, Earth, and the cloud, so that $f_\bullet(0)$ is the fraction of photons removed by a grain that would have otherwise struck Earth.

The cascade of dependencies in this equation begins with the scattering properties of each grain. Its extinction efficiency determines how many Earth-bound solar photons it can eliminate, but that factor, along with the scattering anisotropy, sets β (Eq 23), the degree to which radiation pressure can affect its orbit. Higher values of β require larger distance between the cloud and Earth, substantially reducing the angular size of each dust grain, and diluting the shade provided to Earth. To compensate, the mass of the cloud could be tuned for a desired level of attenuation.

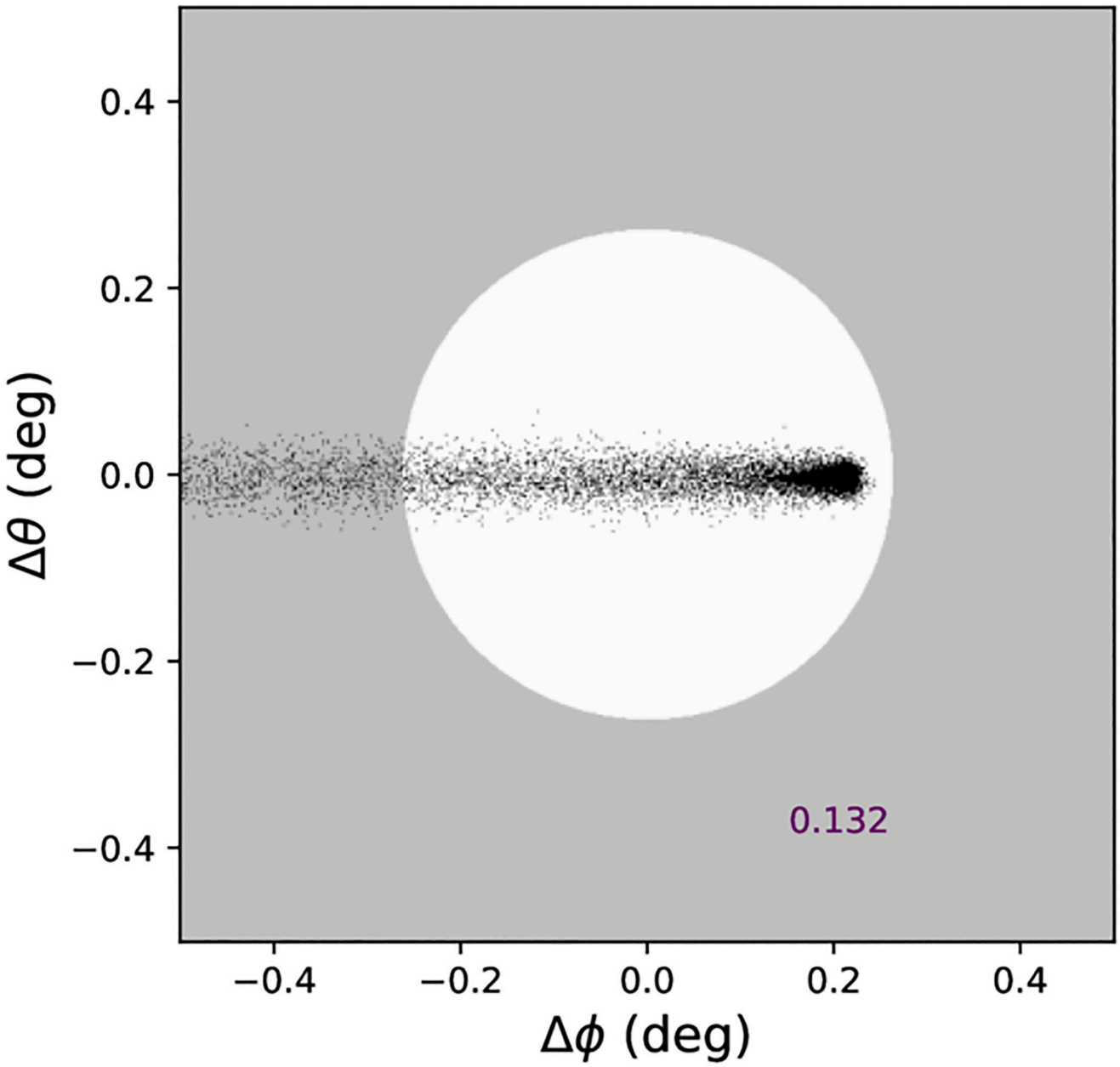

Fig 6. Location of a simulated micron-size grains continuously launched from an orbiter at L_1 in a snapshot as seen from Earth. The viewing location is the subsolar point, and the solid grey circle shows the edge of the solar disk, as in Fig 2. The simulated trajectory of the orbiter is calculated as in that earlier figure. The particles are ejected in a jet-like stream, as described in the text. The image shows grains after 48 days after the start time in the simulation. S1 Animation shows the full sequence of images from which this snapshot was taken.

https://doi.org/10.1371/journal.pclm.0000133.g006

As an alternative to changing the total mass of the cloud to achieve high attenuation, we consider particle size and optical properties. Grains are most efficient scatterers of sunlight when they are around 1 micron in size. Yet micron-size grains typically have high β, possibly to the point where radiation pressure makes these grains unbound to the Sun ($\beta \geq 1$). Material with significant forward scattering, $g \rightarrow 1$, is less susceptible to radiation pressure than back-scatterers. More massive grains, by virtue of increased density or size, have smaller β than less massive ones. Numerical experiments suggest that silicate spheres with $r_p \gtrsim 100\ \mu$m are

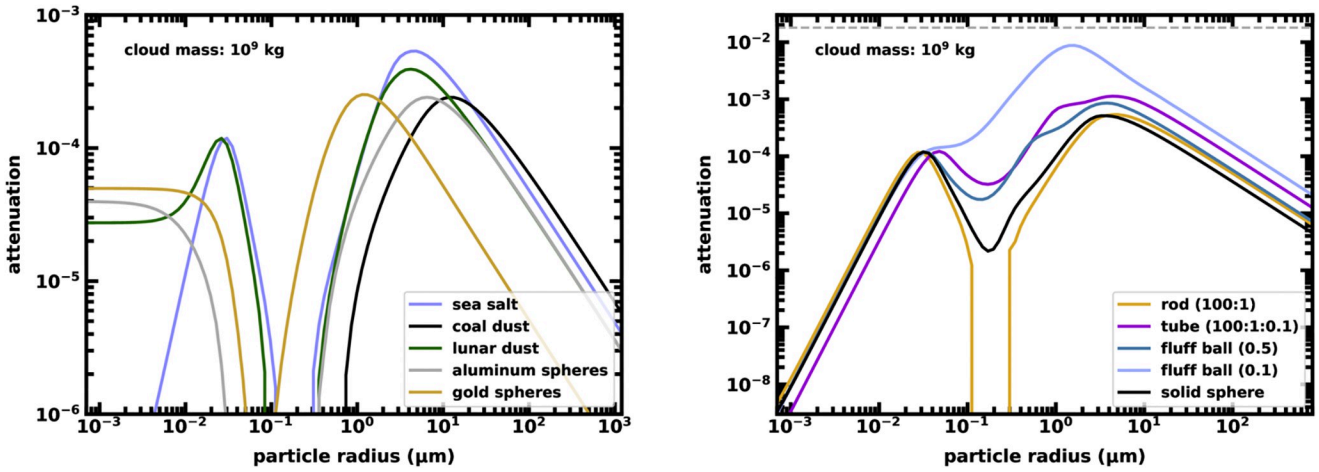

Fig 7. The attenuation from a monodisperse cloud of particles with total mass $M_{\text{cloud}} = 10^9$ kg at an L_1-like location. The panels and curves in this figure correspond to those in Fig 1. Because these clouds corotate with Earth and the Sun for months or longer, the cumulative attenuation is approximately two orders of magnitude greater than the values indicated on the y-axis.

https://doi.org/10.1371/journal.pclm.0000133.g007

massive enough so that radiation pressure does not impact orbits over the course of a year. The down side to this choice is that there are fewer grains for a fixed cloud mass. For a fixed cloud mass, the attenuation generally falls with increasing grain/pebble size.

For sub-micron grains, the extinction efficiency falls with decreasing radius; individual very small particles do not scatter light well. However, they also do not feel much radiation pressure [22], so β is also low, as $d_p \to d_1$. Furthermore, for a fixed cloud mass, the smaller the particles, the more numerous they are. In balance, extinction efficiency, dominated at small particle sizes by absorption in the Rayleigh limit ($Q_{\text{ext}} \to Q_{\text{abs}} \sim r_p$), compensates for the increase in particle number when r_p is reduced. The attenuation from very small grains is independent of grain size for a fixed cloud mass.

Fig 7 illustrates these effects for spherical grains with properties in Table 1 (left panel) as well as the suite of "designer" glass particles in Fig 1 (right panel). The cloud mass is fixed for all materials at $M_{\text{cloud}} = 10^9$ kg. For spherical grains, sea salt seems most promising in the 5–10 μm size range, followed by lunar dust of similar size. While the attenuation is two orders of magnitude lower than the ECI level of 0.025, the persistence of all grains here is roughly a year, so the cumulative attenuation will be close to 0.04 days. Still, the total amount of dust to reach even an attenuation-day must thus exceed 10^{13} g. The availability and location of lunar dust, presumably mined from the lunar surface [18], suggest that this material might be the best choice for generating a massive, persistent cloud at an L_1-like location.

The designer glass grains offer a different scenario. The right panel of Fig 7 shows that a cloud of "fluff balls"—high-porosity glass or aggregates with a filling factor of (0.1)—for example, made from an aggregate of smaller particles—has a cumulative attenuation of approximately 3 days if it remains near d_p for a year. Tubular or rod-like shapes with aspect ratios of $L : D = 100 : 1$, lead to cumulative attenuation around 0.2–0.4 day with 10^9 kg. Substituting aluminum for glass does not substantially change these results.

Numerical experiments highlight that persistence is difficult to achieve even with L_1-like orbits, both in the precision required to initialize them, but also because non-gravitational forces can affect particles of slightly different sizes in significant ways.

Earth-Sun-intercept orbits from the Moon

Because of issues of persistence at L_1 and L_1-like locations, we considered other strategies, including particles launched from the surface of the Moon, on orbits that are optimized to block the Sun as they stream toward L_1. Fig 8 illustrates the path of a burst of lunar dust with

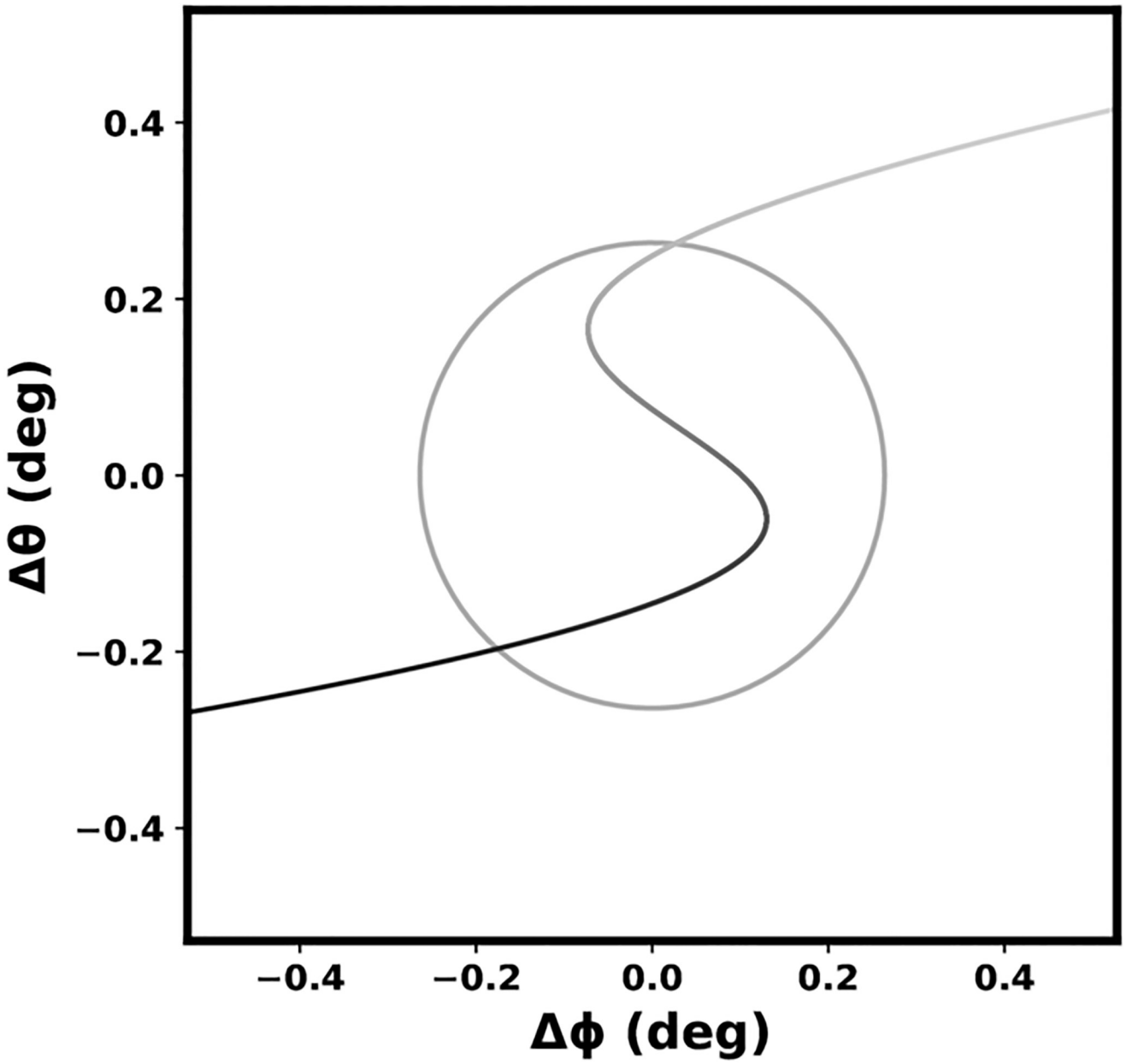

Fig 8. Location of a simulated test particle, launched ballistically from the Moon, crossing the face of the Sun as seen from Earth. The viewing location is the subsolar point, and the solid grey circle shows the edge of the solar disk, as in Fig 2. The simulated trajectory is calculated as in that earlier figure, except that the first hour of the particle's motion was integrated with 400 time steps. The start date in this simulation is April 20, 2022 (JD 2459699.500800758), when the Moon is new. The particle is launched from the Moon's northern pole at a speed of 2.8 km/s relative to the Moon, on a trajectory that reaches close to L_1, and slowly crosses in front of the Sun near the apex of the trajectory (grey points). The grey scale correlates with run time; earlier times have lighter shade. The total time that the particle spends in front of the Sun is about five days.

https://doi.org/10.1371/journal.pclm.0000133.g008

radius 0.2 μm from a ballistic launch at 4.7 km/s from the northern pole of the Moon. The cumulative attenuation in this case is 0.11 days for 10^9 kg of dust.

A similar numerical experiment with larger, 1 μm grains yielded a cumulative attenuation of 0.03 days. Radiation pressure is less impactful than for smaller particles, so these larger grains can achieve an orbit that intercepts Earth and the Sun with slower launch speeds (2.8 km/s). However, despite the longer time that they spend shadowing Earth along their trajectory, their scattering efficiency is relatively low (Fig 1); a cloud of 10^9 kg provides a cumulative attenuation of only 0.025 d.

Fortuitiously, the distribution of grain sizes in the lunar regolith peaks around 0.2 μm, the size with the highest scattering efficiency. In Apollo samples, approximately 20% of the lunar regolith mass is in the form of dust smaller than 20 μm park2008, with a lognormal distribution peaking at a grain size of about 0.2 μm. About 30% of this small-sized material is in grains between 0.1 and 0.3 μm (Fig 3 in [33]). Either sifting the existing regolith for the desired grain size or milling the larger bulk could provide a substantial reservoir of dust. The prospects for mining lunar dust with grain sizes suitable for shielding Earth are promising.

Because of the simplicity of this strategy—a ready source of dust, a ballistic launch with no subsequent orbit corrections—and its low cost in terms of energy compared with a launch from Earth, it could provide a good alternative to maintaining sun-shielding material at L_1.

Energy considerations

Roughly 10^{10} kg of dust per year is needed for Earth-climate impact, which is approximately 700 times more mass than humans have launched into space. A lower bound on the energy requirement of delivering this material comes from the potential difference between the Earth's surface and L_1, $\sim 6.3 \times 10^7$ J/kg. Thus, 10^{10} kg of material for a solar shield from Earth would require close to 10^{18} J, more than the energy spent in 20,000 Saturn V launches.

The potential difference between L_1 and the Moon's surface is about 4% of the L_1-Earth value. From our numerical experiments, launch speeds of 3–5 km/s are needed to send micron-size dust from the Moon on orbits that shade Earth for up to a week. Launching 10^{10} kg of dust at these speeds requires up to 10^{17} J, equivalent to roughly 2500 Saturn V launches. This amount of energy is produced annually by an efficient array of solar panels with an area of less than a few square kilometers. A bank of electromagnetic mass drivers [34, 35], already envisioned for launches from the Moon [36, 37], could place large amounts of dust on Earth-Sun-intercept orbits.

Results and discussion

Toward creating a sun shield with dust, we have explored the attenuation of sunlight received by Earth as a result of an intervening cloud of dust at L_1 or on L_1-like orbits. The new contributions here include the dependence of sun-shading orbits on dust properties and a prescription for launching grains on an L_1-like orbit from the Moon's surface to optimize solar shielding. Table 2 provides a comparison of various materials and launch strategies, and identifies the mass of each material needed to reach a cumulative attenuation of 6 days per year.

We summarize the results with these main points:

- Grains shade Earth most effectively when they are within the L_1 Lagrange point. There, every photon they absorb or deflect is one that would have struck Earth. Serendipitously, grains at L_1 are almost as effective; about 80% of the photons they intercept would have been Earth-bound. Further from Earth, this effectiveness is diminished.

Table 2. Mass requirements for Earth-climate impact of dust clouds.

material[a]	launch[b]	orbit[c]	r_p (μm)	ECI mass[d] (kg)	KE[e] (J)	ref.
coal dust	Earth	L_1	0.17	8.4×10^{10}	6.9×10^{18}	
porous glass	Earth	L_1	0.17	6.6×10^{10}	5.4×10^{18}	
sea salt	Earth	L_1-like	4.9	6.2×10^{10}	5.0×10^{18}	
fluff ball	Earth	L_1-like	1.6	3.6×10^{9}	3.0×10^{17}	
lunar dust	Moon	L_1-like	4.2	8.4×10^{10}	1.1×10^{18}	
lunar dust	Moon	ESI	0.2	5.4×10^{10}	6.0×10^{17}	
lunar dust	Moon	ESI	1.0	2.4×10^{11}	9.4×10^{17}	
solid shield	Earth	L_1	–	10^{11}	10^{19}	[12]
satellite swarm	Earth	L_1	–	2×10^{10}	2×10^{18}	[13]
asteroid dust	NEA	L_1	–	7.6×10^{10}	1.5×10^{17}	[15]
sailcrafts	Earth	L_1	–	3.4×10^{10}	10^{18}	[14]

([a]) The upper section of the table corresponds to dust clouds of materials from Table 1. "Fluff ball" refers to glass with a filling factor of 0.1, as in Fig 1. For comparison, the lower section has estimates for other space-based geoengineering concepts.

([b]) Launch sites include Earth, the Moon, and a near-Earth asteroid (NEA)

([c]) Orbits indicate where sun-shielding occurs, either at Earth-Sun L_1, an L_1-like equilbrium point (Eq 27), or along an Earth-Sun-intercept (ESI) orbit.

([d]) ECI mass is the mass required for a cumulative attenuation of 6 days per year. For L_1-like orbits we assume a persistence of six months. The solid shield, satellite swarm and sailcraft concepts provide shade for multiple years.

([e]) KE is the approximate kinetic energy of the ECI mass at launch, not including transport vehicles.

https://doi.org/10.1371/journal.pclm.0000133.t002

- The details of shading depend on grain size, shape, and composition, all of which determines the extinction efficiency (Q_{ext}). Typically, micron-size grains have higher Q_{ext} than nanoparticles. Breaking up micron-size grains into more numerous smaller particles increases the physical surface area of a cloud, but generally reduces the amount of shade it can provide because of the loss of extinction efficiency. To get the highest level of attenuation $\mathcal{A}$ from a given cloud mass, grains with high porosity are promising, as are particles with large aspect ratios, including cylindrical tubes.
- The effectiveness of a dust cloud as a sun shield depends on how long it can persist between Earth and the Sun before non-gravitational forces disperse it. Persistence of grains at L_1 is low for sizes below 100 microns as a result of radiation pressure and drag from the solar wind. Micron-size grains, if released at L_1, drift away within in a week or so. The persistence time increases with particle mass, as well as the degree to which a grain forward scatters light. For example, micron-size glass that forward scatters feels less radiation pressure than a comparably sized absorber like aluminum or coal dust.
- A strategy to increase persistence of grains at L_1 is to launch them from a platform there at modest speeds (∼10 m/s) to oppose the affect of radiation pressure and solar wind (Fig 6). This method can increase the cumulative attenuation by a factor of two as compared to a dust cloud that is placed at L_1.
- Persistence of smaller grains between Earth and the Sun is enhanced when their orbits are L_1-like, corotating with Earth, but further from Earth than true L_1. At these locations, Earth can shepherd these particles because non-gravitational forces effectively weaken the gravitational influence of the Sun. While L_1-like orbits may be found for a range of grain types, the ones that are closest to the true L_1 are most effective at providing sun shade. A drawback of this strategy for creating a sun shield is that even a small dispersion in grain size (∼1%) can negatively affect persistence.

- The most promising new strategy is to launch lunar grains from the Moon toward L_1. Judiciously chosen trajectories allow streams of grains to shade Earth for up to a week. Because of the availability of optimal-size dust in the lunar regolith, solar energy on the lunar surface, and low escape velocity compared with Earth, this approach may be the most effective for climate-change mitigation of the strategies considered here.

Variations on the choice of materials, launch method, and orbit types may lead to strategies with advantages over the ones considered here. For example, if designer glass grains were manufactured from raw materials on the lunar surface, they may be delivered to an L_1-like orbit more efficiently, or tuned to have mass and scattering properties that enable them to follow Earth-Sun-intercept orbits for longer periods of time than raw lunar dust.

In addition to the *n*-body simulations for estimating persistence and attenuation, we performed extended integrations to confirmed that dust from clouds ejected from the moon or launched between Earth and the Sun do not cross paths with Earth. Once dust is released, its only impact is to shade Earth. It will not otherwise interact with our planet again.

Conclusion

In the scenarios described here, large quantities of dust on orbits between Earth and the Sun can reduce the amount of sunlight received on our planet. Unlike Earth-based strategies, climate-change mitigation with this approach does not have long-term impacts on Earth or its atmosphere. Roughly 10^{10} kg of material annually is needed for Earth-climate impact, depending on the dust properties and how the cloud is deployed. Sources of dust include Earth, the Moon [18], or possibly a deflected asteroid [15, 16, 19]. Because dust grains between Earth and the Sun tend to drift out of alignment, they must be replenished. The lack of control of a dust cloud also may limit its effectiveness as a solar shield. Simulations with controllable sunshades show that a non-uniform shading of Earth may be required to mitigate climate change over the planet as a whole [17]. However, the persistence of dust clouds can be short, allowing for seasonal control of the shading level.

After considering a variety of dust types and deployment strategies, we settle on one scenario as most promising for Earth-climate impact: Lunar dust can be mined and launched on ballistic trajectories that cross near the Earth-Sun line of sight. We have identified orbits that allow dust grains to provide shade for days, almost as long as for dust deployed near L_1, the Earth-Sun Lagrange point. Advantages of this concept include a ready supply of lunar dust, as well as a low kinetic energy cost as compared to an Earth launch. Individual dust grains on these trajectories rapidly drift out of alignment, clearing the Earth-Moon system with no impact on Earth's atmosphere. There is no need to actively manipulate orbits to remove dust when sun shielding is no longer beneficial.

Other space-based geoengineering concepts, including satellite-swarm operations [13, 14] and the space bubble platform from MIT's Senseable City Lab, move less mass over time. We nonetheless urge consideration of a Moon launch and orbits similar to the ones identified here. This strategy requires an order of magnitude less energy than Earth launches. Once Moon-based launch facilities are established, large amounts of dust could be uploaded quickly and continuously, factors that could be essential if humans do not correct course on climate change.

Supporting information

S1 Table. Initial conditions for simulations of orbits at L_1 and Moon launches. Data the Sun and the planets listed are from the NASA JPL Horizons ephemirides server for April 20,

2022 (JD 2459699.500800758). The "L_1" row corresponds to the simulation in Fig 2 for an object at L_1 (gravity only, no radiation pressure or forces from the solar wind). The "lunar dust" row contains data corresponding to the trajectory in Fig 8, a launch of 0.2 μm dust from the Moon on an Earth-Sun-intercept orbit. For all n-body integrations, we use the masses of the Sun and the planets provided by Horizons, adopting a Newton constant of 6.67403×10^{-11} $N \cdot m^2/kg^2$. Source code for performing these integrations (as well as other calculations) is available at `https://github.com/benjbromley/Dust-as-a-solar-shield`. (PDF)

S1 Animation. A simulation of dust launched from a platform orbiting at L_1. The animation shows the paths of dust ejected at 10 m/s in a stream with a dispersion of 0.1 m/s, directed at an angle $\theta_v = 65^\circ$ relative to the Earth's direction of travel. The number in the lower right is the time in years since the start of the simulation. Fig 6 is a snapshot from this sequence. (GIF)

Acknowledgments

We are grateful for helpful discussions with M. Geller. Guidance and encouragement from I., R., and M. Bromley-Dulfano, S. Limon, Z. Y. Kang, SDB and PRB were also appreciated. The comments from several reviewers significantly improved the presentation. S. Khan acknowledges support from the University of Utah through the Undergraduate Research Opportunity Program.

Author Contributions

Conceptualization: Benjamin C. Bromley, Sameer H. Khan, Scott J. Kenyon.

Formal analysis: Benjamin C. Bromley, Sameer H. Khan, Scott J. Kenyon.

Investigation: Benjamin C. Bromley, Sameer H. Khan, Scott J. Kenyon.

Methodology: Benjamin C. Bromley, Sameer H. Khan, Scott J. Kenyon.

Project administration: Benjamin C. Bromley.

Software: Benjamin C. Bromley.

Supervision: Benjamin C. Bromley.

Visualization: Benjamin C. Bromley.

Writing – original draft: Benjamin C. Bromley, Scott J. Kenyon.

Writing – review & editing: Benjamin C. Bromley, Sameer H. Khan, Scott J. Kenyon.

References

1. Lenton TM, Held H, Kriegler E, Hall JW, Lucht W, Rahmstorf S, et al. Tipping elements in the Earth's climate system. Proceedings of the National Academy of Sciences. 2008; 105(6):1786–1793. https://doi.org/10.1073/pnas.0705414105 PMID: 18258748
2. Masson-Delmotte V, Zhai P, Pörtner HO, Roberts D, Skea J, Shukla P, et al. Global warming of 1.5˚C: Summary for policy makers. IPCC—The Intergovernmental Panel on Climate Change; 2018.
3. Lenton T, Rockström J, Gaffney O, Rahmstorf S, Richardson K, Steffen W, et al. Climate tipping points—too risky to bet against. Nature. 2019; 575:592–595. https://doi.org/10.1038/d41586-019-03595-0 PMID: 31776487
4. Caldeira K, Bala G, Cao L. The Science of Geoengineering. Annual Review of Earth and Planetary Sciences. 2013; 41:231–256. https://doi.org/10.1146/annurev-earth-042711-105548

5. Govindasamy B, Caldeira K. Geoengineering Earth's radiation balance to mitigate CO_2-induced climate change. Geophysical Research Letters. 2000; 27(14):2141–2144. https://doi.org/10.1029/1999GL006086
6. Kravitz B, Caldeira K, Boucher O, Robock A, Rasch PJ, Alterskjær K, et al. Climate model response from the Geoengineering Model Intercomparison Project (GeoMIP). Journal of Geophysical Research (Atmospheres). 2013; 118(15):8320–8332. https://doi.org/10.1002/jgrd.50646
7. Li J, Carlson BE, Yung YL, Lv D, Hansen J, Penner JE, et al. Scattering and absorbing aerosols in the climate system. Nature Reviews Earth and Environment. 2022; 3(6):363–379. https://doi.org/10.1038/s43017-022-00296-7
8. National Research Council. Climate Intervention: Reflecting Sunlight to Cool Earth. Washington, DC: The National Academies Press; 2015. Available from: https://nap.nationalacademies.org/catalog/18988/climate-intervention-reflecting-sunlight-to-cool-earth.
9. IPCC. Climate Change 2022: Mitigation of Climate Change. Contribution of Working Group III to the Sixth Assessment Report of the Intergovernmental Panel on Climate Change. Cambridge, UK and New York, NY, USA: Cambridge University Press; 2022.
10. Early JT. Space-based solar shield to offset greenhouse effect. Journal of the British Interplanetary Society. 1989; 42:567–569.
11. Hudson HS. A Space Parasol as a Countermeasure Against the Greenhouse Effect. Journal of the British Interplanetary Society. 1991; 44:139.
12. McInnes CR. Minimum Mass Solar Shield for Terrestrial Climate Control. Journal of the British Interplanetary Society. 2002; 55:307–311.
13. Angel R. Feasibility of cooling the Earth with a cloud of small spacecraft near the inner Lagrange point (L1). Proceedings of the National Academy of Sciences. 2006; 103(46):17184–17189. https://doi.org/10.1073/pnas.0608163103 PMID: 17085589
14. Fuglesang C, de Herreros Miciano MG. Realistic sunshade system at L_1 for global temperature control. Acta Astronautica. 2021; 186:269–279. https://doi.org/10.1016/j.actaastro.2021.04.035
15. Bewick R, Sanchez JP, McInnes CR. The feasibility of using an L_1 positioned dust cloud as a method of space-based geoengineering. Advances in Space Research. 2012; 49(7):1212–1228. https://doi.org/10.1016/j.asr.2012.01.010
16. Bewick R, Sanchez JP, McInnes CR. Gravitationally bound geoengineering dust shade at the inner Lagrange point. Advances in Space Research. 2012; 50(10):1405–1410. https://doi.org/10.1016/j.asr.2012.07.008
17. Sánchez JP, McInnes CR. Optimal Sunshade Configurations for Space-Based Geoengineering near the Sun-Earth L1 Point. PLoS ONE. 2015; 10(8):e0136648. https://doi.org/10.1371/journal.pone.0136648 PMID: 26309047
18. Struck C. The Feasibility of Shading the Greenhouse with Dust Clouds at the Stable Lunar Lagrange Points. Journal of the British Interplanetary Society. 2007; 60:82–89.
19. Pearson J, Oldson J, Levin E. Earth rings for planetary environment control. Acta Astronautica. 2006; 58(1):44–57. https://doi.org/10.1016/j.actaastro.2005.03.071
20. Salazar FJT, McInnes CR, Winter OC. Intervening in Earth's climate system through space-based solar reflectors. Advances in Space Research. 2016; 58(1):17–29. https://doi.org/10.1016/j.asr.2016.04.007
21. Salazar FJT, Prado AFBA. Sun-synchronous orbital dust ring to reduce climate change at the polar caps. European Physical Journal Plus. 2022; 137(6):710. https://doi.org/10.1140/epjp/s13360-022-02866-6
22. Burns JA, Lamy PL, Soter S. Radiation forces on small particles in the solar system. Icarus. 1979; 40(1):1–48.
23. Berg MJ, Sorensen CM, Chakrabarti A. A new explanation of the extinction paradox. Journal of Quantitative Spectroscopy and Radiative Transfer. 2011; 112:1170–1181. https://doi.org/10.1016/j.jqsrt.2010.08.024
24. Schlichting HE, Ofek EO, Sari R, Nelan EP, Gal-Yam A, Wenz M, et al. Measuring the Abundance of Sub-kilometer-sized Kuiper Belt Objects Using Stellar Occultations. Astrophysical Journal. 2012; 761(2):150. https://doi.org/10.1088/0004-637X/761/2/150
25. hlaing M, Gebear-Eigzabher B, Roa A, Marcano A, Radu D, Lai CY. Absorption and scattering cross-section extinction values of silver nanoparticles. Optical Materials. 2016; 58:439–444. https://doi.org/10.1016/j.optmat.2016.06.013
26. Fabian D, Henning T, Jäger C, Mutschke H, Dorschner J, Wehrhan O. Steps toward interstellar silicate mineralogy. VI. Dependence of crystalline olivine IR spectra on iron content and particle shape. Astronomy and Astrophysics. 2001; 378:228–238. https://doi.org/10.1051/0004-6361:20011196

27. Gordon HR. Light scattering and absorption by randomly-oriented cylinders: dependence on aspect ratio for refractive indices applicable for marine particles. Opt Express. 2011; 19(5):4673–4691. https://doi.org/10.1364/OE.19.004673 PMID: 21369299

28. Kenyon SJ, Bromley BC. Variations on Debris Disks III. Collisional Cascades and Giant Impacts in the Terrestrial Zones of Solar-type Stars. Astrophysical Journal. 2016; 817(1):51. https://doi.org/10.3847/0004-637X/817/1/51

29. Bromley BC, Kenyon SJ. A Hybrid N-Body-Coagulation Code for Planet Formation. Astronomical Journal. 2006; 131(5):2737–2748. https://doi.org/10.1086/503280

30. Beauge C, Ferraz-Mello S. Capture in Exterior Mean-Motion Resonances Due to Poynting-Robertson Drag. Icarus. 1994; 110(2):239–260. https://doi.org/10.1006/icar.1994.1119

31. Liou JC, Zook HA, Jackson AA. Radiation Pressure, Poynting-Robertson Drag, and Solar Wind Drag in the Restricted Three-Body Problem. Icarus. 1995; 116(1):186–201. https://doi.org/10.1006/icar.1995.1120

32. Klačka J, Petržala J, Pástor P, Kómar L. Solar wind and the motion of dust grains. Monthly Notices of the Royal Astronomical Society. 2012; 421(2):943–959. https://doi.org/10.1111/j.1365-2966.2012.20321.x

33. Park J, Liu Y, Kihm KD, Talyor LA. Characterization of Lunar Dust for Toxicological Studies. I: Particle Size Distribution. Journal of Aerospace Engineering. 2008; 21(4):266–271. https://doi.org/10.1061/(ASCE)0893-1321(2008)21:4(266)

34. Apel U. Possibilities and limits of electromagnetic acceleration in space applications; 1984. Thesis Technische Univ., Berlin (Germany, F.R.). Inst. für Luft- und Raumfahrt.

35. Cowan M, Widner MM, Cnare EC, Duggin BW, Kaye RJ, Freeman JR. Exploratory development of the reconnection launcher 1986-90. IEEE Transactions on Magnetics. 1991; 27(1):563–567. https://doi.org/10.1109/20.101095

36. Bilby C, Davis H, Nozette S, Driga M, Kamm R. A Lunar Electromagnetic Launcher. In: Second Conference on Lunar Bases and Space Activities of the 21st Century. vol. 652 of LPI Contributions; 1988. p. 21.

37. Snow WR, Kolm HH. Electromagnetic Launch of Lunar Material. In: McKay MF, McKay DS, Duke MB, editors. Space resources. vol. 509. NASA; 1992. p. 117.